Cell Calcium 120 (2024) 102883

Contents lists available at ScienceDirect

Cell Calcium

journal homepage: www.elsevier.com/locate/ceca

# Simultaneous TIRF imaging of subplasmalemmal $Ca^{2+}$ dynamics and granule fusions in insulin-secreting INS-1 cells reveals coexistent synchronized and asynchronous release

Charlotte Suckert [1], Carolin Zosel [1], Michael Schaefer [*]

*Leipzig University, Rudolf-Boehm-Institute of Pharmacology and Toxicology, Härtelstraße 16-18, Leipzig 04107, Germany*

ARTICLE INFO

*Keywords:*
L-type $Ca_v$ channel
Insulin release
$Ca_v$ 1.2
$Ca_v$ 1.3
Pancreatic beta cells
$Ca^{2+}$ signalling
Secretion coupling

ABSTRACT

The basal and glucose-induced insulin secretion from pancreatic beta cells is a tightly regulated process that is triggered in a $Ca^{2+}$-dependent fashion and further positively modulated by substances that raise intracellular levels of adenosine 3′,5′-cyclic monophosphate (cAMP) or by certain antidiabetic drugs. In a previous study, we have temporally resolved the subplasmalemmal $[Ca^{2+}]_i$ dynamics in beta cells that are characterized by trains of sharply delimited spikes, reaching peak values up to 5 μM. Applying total internal reflection fluorescence (TIRF) microscopy and synaptopHluorin to visualize fusion events of individual granules, we found that several fusion events can coincide within 50 to 150 ms. To test whether subplasmalemmal $[Ca^{2+}]_i$ microdomains around single or clustered $Ca^{2+}$ channels may cause a synchronized release of insulin-containing vesicles, we applied simultaneous dual-color TIRF microscopy and monitored $Ca^{2+}$ fluctuations and exocytotic events in INS-1 cells at high frame rates. The results indicate that fusions can be triggered by subplasmalemmal $Ca^{2+}$ spiking. This, however, does account for a minority of fusion events. About 90 %-95 % of fusion events either happen between $Ca^{2+}$ spikes or incidentally overlap with subplasmalemmal $Ca^{2+}$ spikes. We conclude that only a fraction of exocytotic events in glucose-induced and tolbutamide- or forskolin-enhanced insulin release from INS-1 cells is tightly coupled to $Ca^{2+}$ microdomains around voltage-gated $Ca^{2+}$ channels.

## 1. Introduction

A well-characterized bursting electrical activity in glucose-stimulated beta cells is driven by voltage-gated $Na^+$, $Ca^{2+}$ and $K^+$ channels that are modulated by a plethora of up- and downstream mechanisms [1] leading to oscillatory fluctuations of the intracellular $Ca^{2+}$ concentration ($[Ca^{2+}]_i$). By facilitating membrane depolarisation, the glucose- or drug-dependent closure of $K_{ATP}$ channels induces or accelerates the frequency of electrical continuous firing. Activation of $G_s$-protein-coupled receptors e.g. by the incretins gastric inhibitory peptide (GIP) or glucagon-like peptide 1 (GLP-1) [2,3], and stimulation of $G_q$-protein-coupled muscarinic acetylcholine or free fatty acid receptors [4,5] further increase the beta cell activity either by enhancing $Ca^{2+}$ signalling or by facilitating the priming and docking of insulin-containing granules.

The insulin release from isolated Langerhans islets is long known to be organised as a pulsatile phenomenon, which occurs synchronized to waves of intracellular $Ca^{2+}$ elevations [6,7]. With typical frequencies in the range of 0.1–2 $min^{-1}$, these waves are too slow to reflect the output of single action potentials, but they may result from grouped trains or bursts of action potentials, each [8]. Electrophysiological studies have clearly demonstrated that sub-second depolarising pulses or flash photolysis of intracellularly loaded caged $Ca^{2+}$ trigger fast increases in the membrane capacitance in beta cells or in beta cell-derived

*Abbreviations:* $[Ca^{2+}]_i$, intracellular $Ca^{2+}$ concentration; BAPTA, 1,2-bis (o-aminophenoxy) ethane-N,N,N′,N′-tetraacetic acid; cAMP, adenosine 3′,5′-cyclic monophosphate; $Ca_V$, voltage-gated $Ca^{2+}$ channel; EGTA, ethylene glycol-bis (β-aminoethyl ether)-N,N,N′,N′-tetraacetic acid; EPAC, exchange protein directly activated by cAMP; GIP, gastric inhibitory peptide; GFP, enhanced green fluorescent protein; GLP-1, glucagon-like peptide 1; KRHB, krebs-ringer-henseleit buffer; qCMOS, quantitative complementary metal-oxide-semiconductor; PKCα, protein kinase C α; RFP, monomeric red fluorescent protein; RRP, readily releasable pool; Syt, synaptotagmin; TIRF, total internal reflection fluorescence.

* Corresponding author.
*E-mail address:* michael.schaefer@medizin.uni-leipzig.de (M. Schaefer).

[1] These authors contributed equally to this work.

https://doi.org/10.1016/j.ceca.2024.102883
Received 4 January 2024; Received in revised form 21 March 2024; Accepted 29 March 2024
Available online 8 April 2024

immortalized cell lines, including INS-1 cells [9–11]. These findings, along with amperometric analyses demonstrated the existence of a readily releasable pool (RRP), which engages in a $Ca^{2+}$-dependent fashion [12,13]. In a recent study applying low affinity $Ca^{2+}$ indicator dyes and total internal reflection fluorescence (TIRF) microscopy, we have demonstrated that subplasmalemmal $Ca^{2+}$ spikes can reach frequencies of 2–8 Hz and subplasmalemmal peak $Ca^{2+}$ concentrations of up to 5 μM (Langlhofer et al. [14]). These concentrations might be sufficient to locally activate $Ca^{2+}$ sensors, such as high- to medium-affinity synaptotagmins (Syt) within $Ca^{2+}$ microdomains around single or locally clustered $Ca_V$ channels. Candidate isotypes that are expressed in beta cells and in insulin-secreting cell lines include the high affinity isoforms Syt3, Syt5 and Syt7 (see [15] and references therein). Moreover, endocrine pancreatic cells not only express core proteins required for exocytosis, such as VAMP2, syntaxin 1A and SNAP-25, but also proteins that qualify as active zone proteins, such as Munc13–1, Munc-18, ELKS, Piccolo, Bassoon, RIM2a, and complexin 2 [16–18]. Despite the lack of a direct correlate of presynaptic active zones, beta cells might physically link a subpool of insulin granules to voltage-gated $Ca^{2+}$ channels and thereby position them within a $Ca^{2+}$ nanodomain around the pore mouth (tight coupling).

Although all components of rapid $Ca^{2+}$-triggered exocytosis are in place, an active zone-like domain may control only a fraction of insulin release [19]. Another fraction of insulin granule release would be controlled by PLC-mediated $Ca^{2+}$ mobilisation from internal inositol 1,4, 5-trisphosphate ($InsP_3$)-sensitive stores and $Ca^{2+}$/calmodulin-dependent kinase II (CaMK-II)-mediated protein phosphorylation, cAMP-dependent priming of granules or other hormonally induced intracellular signalling cascades [1,20]. Such coupling mechanisms may either serve to prime granules for subsequent $Ca^{2+}$-triggered synchronized release or result in a temporally asynchronous and spatially loose coupling between $Ca^{2+}$ signalling and release events, as shown for $Ca^{2+}$-induced exocytosis from bovine adrenal chromaffin cells [21].

We wondered whether and to what percentage exocytosis events are acutely triggered by and synchronized with $Ca^{2+}$ spikes in the subplasmalemmal compartment during opening of voltage-gated $Ca^{2+}$ channels in non-disturbed resting and stimulated cells. To investigate this process with sufficient spatial and temporal resolution, we applied high-speed dual-color TIRF microscopy in INS-1 cells that heterologously expressed genetically encoded markers to simultaneoulsy observe increases in $[Ca^{2+}]_i$ and exocytosis of individual granules. In case of direct $Ca^{2+}$-triggered exocytosis, we expected that $Ca^{2+}$ spikes and release events should temporally coincide. To achieve the necessary sensitivity and temporal resolution, suitable combinations of fluorescent biosensors were identified, and a statistical model was developed to assess the fractions of directly $Ca^{2+}$-triggered versus asynchronous exocytotic events in resting and in glucose- or drug-stimulated INS-1 cells.

## 2. Results

### 2.1. Glucose-induced $Ca^{2+}$ spiking and coincidence of vesicle fusions in INS-1 cells

As previously described by Langlhofer et al. [14], INS-1 cells loaded with the low affinity $Ca^{2+}$indicator Cal520ff ($K_D$ = 9.8 μM, $\lambda_{ex}$ = 493 nm, $\lambda_{em}$ = 515 nm) showed glucose-induced fast subplasmalemmal $Ca^{2+}$ spiking with peak frequencies of 2–8 Hz (Fig. 1A, B). Different $Ca^{2+}$ spiking dynamics were observed, such as isolated single spikes or burst-like patterns with and without intermitting return to baseline levels (Fig. 1B).

Since subplasmalemmal $Ca^{2+}$ spikes in INS-1 cells are highly synchronized within single cells, we reasoned that a $Ca^{2+}$-triggered exocytotic release of insulin-containing granules may result in synchronous release of more than a single vesicle. Indeed, by visualizing synaptopHluorin-expressing INS-1 cells via TIRF microscopy, coinciding exocytotic vesicle fusions with the plasma membrane were eventually observed within a time interval of 150 ms or less (Fig. 1C, D). We therefore formulated the hypothesis that the release of insulin-containing vesicles may rely on subplasmalemmal $Ca^{2+}$ microdomains that reach peak $Ca^{2+}$ concentrations of 2–5 μM [14]. To assess whether ryanodine receptor- or inositol-1,4,5-trisphosphate receptor-mediated $Ca^{2+}$ mobilization events contribute to these subplasmalemmal $Ca^{2+}$ fluctuations, cells were pre-treated with 2 μM thapsigargin. Spike amplitudes as well as spike frequencies in thapsigargin-treated cells did not differ significantly from those observed in untreated controls (Suppl. Fig. S1). Thus, the subplasmalemmal $Ca^{2+}$ spiking almost exclusively reflects influx events, which are presumably mediated by voltage-gated $Ca^{2+}$ channels that open and close in synchronicity with the electrical oscillator. To study the role of $Ca^{2+}$ microdomains around voltage-gated $Ca^{2+}$ channels for exocytosis in more detail, we performed a set of experiments in thapsigargin-treated INS-1 cells with and without additional intracellular loading of $Ca^{2+}$ buffers. When pre-loaded with a concentration of 10 μM EGTA-AM, cells showed a diminished amplitude and spatial spread of subplasmalemmal $Ca^{2+}$ signals, indicating remaining subplasmalemmal $Ca^{2+}$ microdomains (Suppl. Fig. S2). Using higher concentrations, the spatial spread became smaller, and after pre-loading with 30 μM EGTA-AM, no $Ca^{2+}$ signals were detectable with Cal520ff, indicating efficient global buffering. Under the same experimental conditions, fusion rates reported in synaptopHluorin-expressing cells dropped by about 23.3 % (Fig. 1E), whereas pre-loading with 30 μM BAPTA-AM caused a stronger (44.8 %) and statistically significant decrease of fusion rates (Fig. 1E). When monitored in a $Ca^{2+}$-free buffer, fusion rates were further diminished about 57.4 % (Fig. 1E).

In most INS-1 cells, the entire cell bottom was spiking, pointing to a channel density that causes confluence of subplasmalemmal $Ca^{2+}$ signals within less than 20 ms. In a few INS-1 cells, a lower channel density was apparent, allowing the experimental analysis of sparklets originating from a single channel or channel cluster (Fig. 2A). In 48 consecutive sparklets observed within 20 s, the time-to-peak was 18.1 ± 5.1 ms (mean ± *S*.D.) with a fastest and slowest upstroke within 6 ms and 26 ms, respectively. Here, the microdomain reached a central peak concentration of 4–5 μM, and broadened with a lateral spread of more than 1.5 μm within 2 ms (Fig. 2B-D). Thus, isolated or confluent $Ca^{2+}$microdomains could reach concentrations that are sufficient to engage high affinity synaptotagmins [22] and thereby trigger a synchronized release of granules.

As an alternative hypothesis, coincident fusions of two or more vesicles may simply represent stochastic events that appear more frequent during episodes of generally high exocytotic activity. To investigate the correlation between $Ca^{2+}$ spikes and exocytosis more directly, a simultaneous co-imaging of the $Ca^{2+}$ dynamics and fusion events with two different fluorophores was established. Because pHluorins are only available as green emitting fluorescent proteins ($\lambda_{ex}$=475 nm, $\lambda_{em}$=510 nm [23]), a red emitting $Ca^{2+}$indicator that is capable of reporting subplasmalemmal $Ca^{2+}$ fluctuations in high-speed TIRF microscopy was required.

### 2.2. Comparison of different red emitting $Ca^{2+}$indicators with the green emitting Cal520ff

Since Cal520ff was carefully selected as green emitting $Ca^{2+}$ indicator dye that suited our demands in $Ca^{2+}$ microdomain imaging best (with alternative indicators that failed for several reasons), we were aware of possible problems that are associated with specific indicator dyes or genetically encoded biosensors. Therefore, red $Ca^{2+}$ indicators were compared to signals recorded with Cal520ff by simultaneous dual-color TIRF microscopy. First, the commercially available X-Rhod-1-AM ($\lambda_{ex}$ = 580 nm, $\lambda_{em}$ = 602 nm, $K_D$ = 0.7 μM) was tested (Fig. 3A, B). In contrast to Cal520ff, X-Rhod-1 tends to accumulate in mitochondria (Fig. 3A; [25]). Additionally, it did not faithfully represent every single $Ca^{2+}$spike indicated by Cal520ff (Fig. 3B). Most importantly, however,

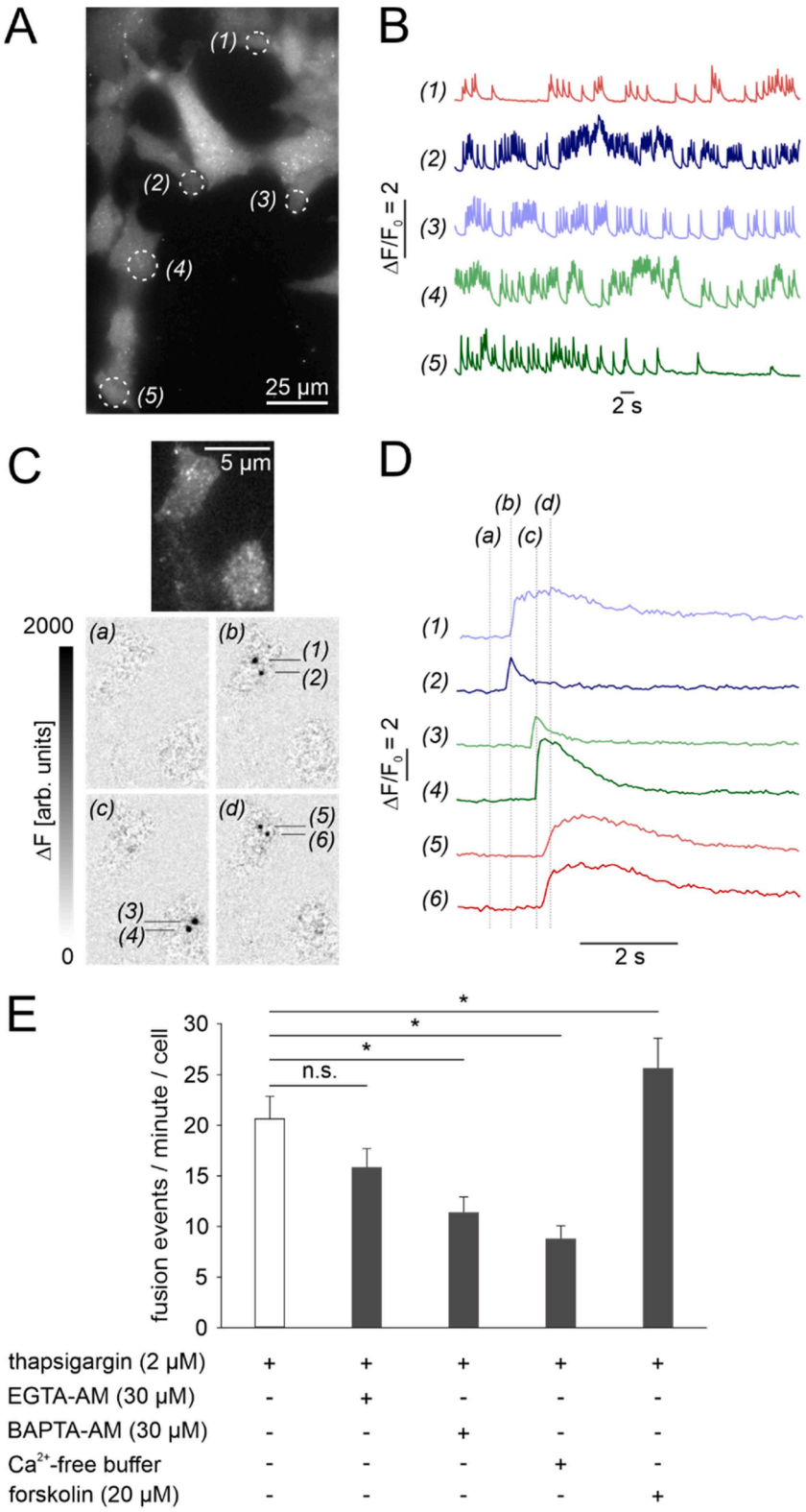


*(caption on next page)*

**Fig. 1.** Subplasmalemmal $Ca^{2+}$ fluctuations and vesicle fusions in INS-1 cells visualized by TIRF microscopy. INS-1 cells loaded with the low affinity $Ca^{2+}$ indicator Cal520ff **(A, B)** or INS-1 cells expressing synaptopHluorin **(C, D)** were kept in KRHB solution, supplemented with 15 mM glucose and images were acquired every 50 ms (20 Hz) with an excitation wavelength of 475 nm. **(A)** The image shows raw data in Cal520ff-loaded INS-1 cells. **(B)** Time course of fluorescence changes in individual cells corresponding to the ROIs depicted in **(A). (C)** Images represent raw data (upper image) or fluorescence changes (ΔF) within 150 ms (a-d). A sudden appearance of spots marked as *(1)-(6)* indicates individual fusion events. **(D)** Time course of fluorescence changes detected over regions of interest (ROI) defined at positions of individual fusion events as indicated in **(C). (E)** Analysis of the impact of $Ca^{2+}$ influx on fusion rates in INS-1 cells exposed to 15 mM glucose. Fusion events were monitored as shown in **(C, D)** for 50–100 s, and expressed as fusions $min^{-1}$ $cell^{-1}$. To assess the impact of intracellular $Ca^{2+}$ buffering, INS-1 cells were loaded with EGTA-AM or BAPTA-AM (30 μM each) for 30 min prior to the experiments. A contribution of $Ca^{2+}$ mobilization events was excluded by pre-treating cells with 2 μM thapsigargin for 10–15 min. Cells were either kept in $Ca^{2+}$-containing KRHB or in nominally $Ca^{2+}$-free KRHB supplemented with 0.5 mM EGTA as indicated ($n_{thapsigargin} = 86$ cells, $n_{EGTA\text{-}AM} = 44$ cells, $n_{BAPTA\text{-}AM} = 34$ cells, $n_{Ca2+\text{-}free\ buffer} = 68$ cells, $n_{forskolin} = 43$ cells. Statistical analysis was performed using the *t*-test for parametric unpaired data, normal distribution of the data was tested with the Kolmogorov-Smirnov test or the Wilcoxon-Mann-Whitney test for non-parametric unpaired data, $*p \leq 0.05$, bars: means and S.E.).

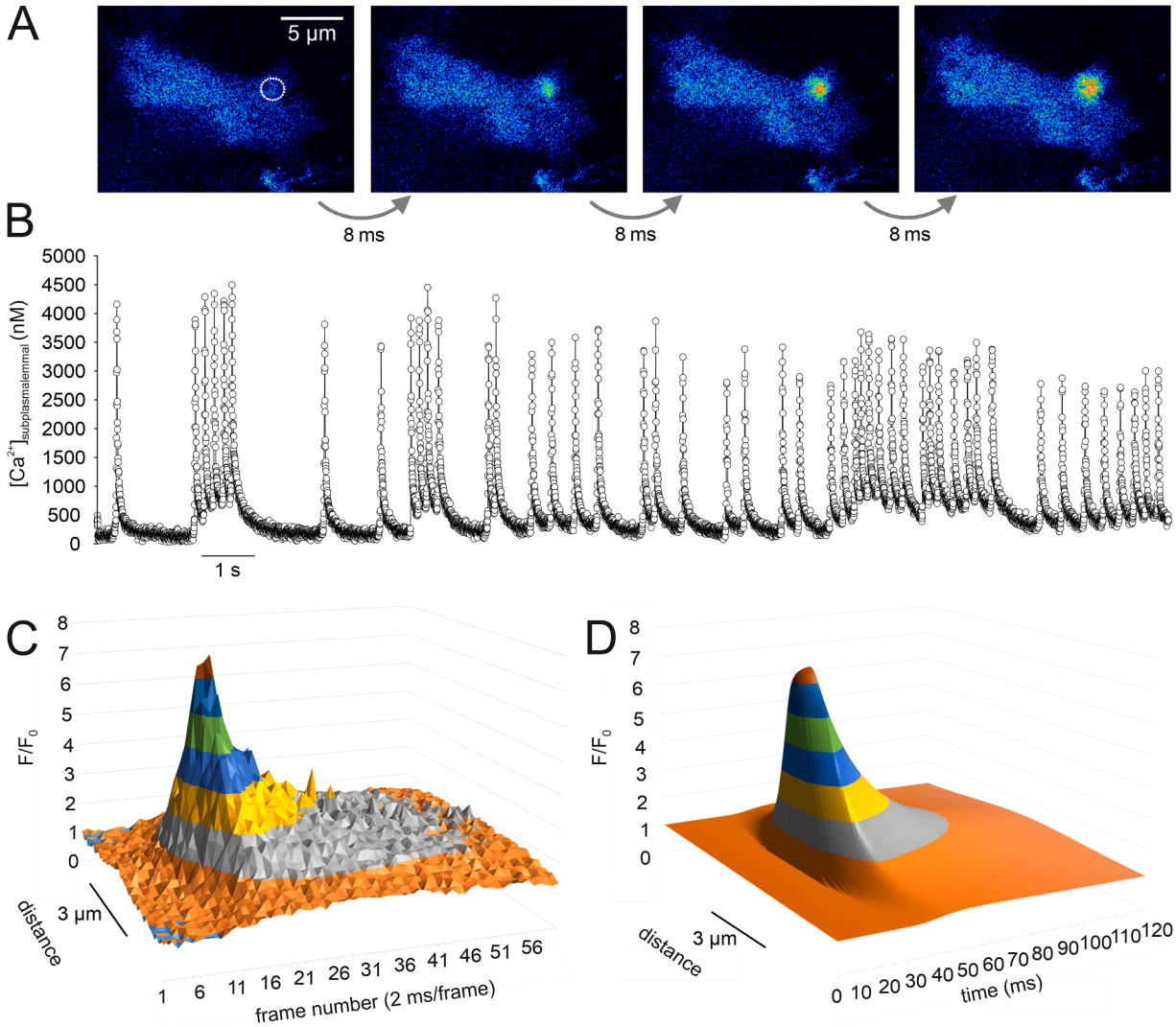


**Fig. 2.** Spatiotemporally resolved $Ca^{2+}$ microdomain spiking in a Cal520ff-loaded INS-1 cell stimulated with 15 mM glucose. TIRF microscopic images of a single spiking INS-1 cell were obtained at a frame rate of 500 Hz. **(A)** Background-corrected raw fluorescence intensity data before and during the development of a $Ca^{2+}$sparklet. **(B)** Time course of apparent $[Ca^{2+}]_i$ in the subplasmalemmal ROI marked in **(A). (C)** Kymograph presentation of a single $Ca^{2+}$ sparklet as measured in **(B)**. The 3 μm-bar depicts the radial distance from the center of the sparklet. Data is depicted as $F/F_0$ during a 120-ms time span. **(D)** Computer-simulated idealized indicator response in a microdomain, assuming a single $Ca^{2+}$ channel opening. $I_{Ca} = 100$ fA, $t_{open} = 12$ ms, 50 % $Ca^{2+}$ binding to high mobility buffers ($D = 110$ $\mu m^2/s$; [24]) and medium mobility buffers ($D = 20$ $\mu m^2/s$), each. For sequestration of $[Ca^{2+}]_i$, a $k_{off} = 8$ $s^{-1}$ was assumed.

excitation of X-Rhod-1 caused a cessation of $Ca^{2+}$influx events in INS-1 cells within 20–60 s in most experiments (Fig. 3B). Shortening the exposure times, dimming the light source, or reducing the concentration of X-Rhod-1-AM during dye loading only partially relieved the effect, but caused an unacceptable drop of the signal-to-noise ratio with failure to reliably detect the upstroke time of single $Ca^{2+}$ spikes. This effect appears to be specific for X-Rhod-1, because none of the other investigated red emitting indicators (CAR-GECO1, PKC$\alpha_{mCherry2}$) stalled the glucose-induced $Ca^{2+}$ spiking upon excitation with the same wavelength and comparable intensities (Fig. 3D, F).

The genetically encoded high affinity $Ca^{2+}$indicator CAR-GECO1 ($\lambda_{ex}$ = 562 nm, $\lambda_{em}$ = 609 nm, $K_D$ = 0.49 μM; [26]) was examined next

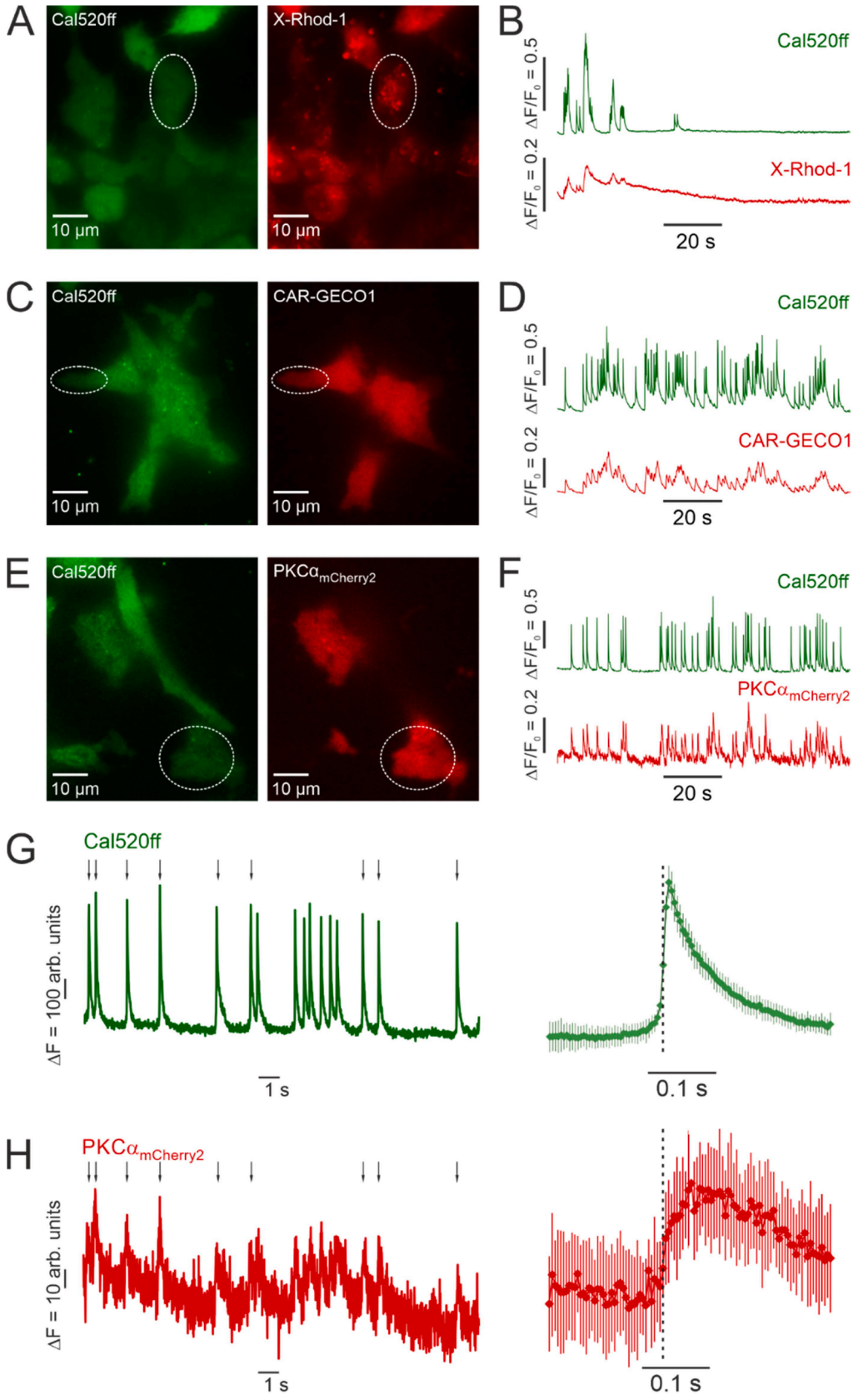


*(caption on next page)*

**Fig. 3.** PKCα$_{mCherry2}$ but not X-Rhod-1 or CAR-GECO1 faithfully reports subplasmalemmal $Ca^{2+}$ spikes. **(A)** Images depict raw data of INS-1 cells intracellularly co-loaded with the low affinity $Ca^{2+}$ indicator Cal520ff (green) and the high affinity $Ca^{2+}$ indicator X-Rhod-1 (red). **(B)** Time course of fluorescence changes detected in the highlighted ROI in **(A)**. **(C)** Raw data images show INS-1 cells intracellularly loaded with Cal520ff (green) and expressing the genetically encoded high affinity $Ca^{2+}$ indicator CAR-GECO1 (red). **(D)** Time course of fluorescence changes measured in the highlighted ROI in **(C)**. **(E)** Images represent raw data of INS-1 cells intracellularly loaded with Cal520ff (green) and expressing PKCα$_{mCherry2}$ (red) as $Ca^{2+}$indicator. **(F)** Temporal fluorescence changes detected in the highlighted ROI in **(E)**. Simultaneous dual-color TIRF microscopy images were acquired every 50 ms (20 Hz). **(G, H)** Time course of fluorescence changes in an intracellularly Cal520ff loaded **(G)** and PKCα$_{mCherry2}$ expressing **(H)** INS-1 cell with an acquisition time of 4 ms (250 Hz). The right panels show an averaged signal consisting of the marked signals in the left panels (arrowheads). Data represent means ± SD (n = 9).

(Fig. 3D, E). Although it reported more of the Cal520ff indicated $Ca^{2+}$upstrokes than X-Rhod-1 did, it could not resolve upstrokes that were superimposed on elevated $Ca^{2+}$ levels (Fig. 3D), an effect that presumably results from saturated $Ca^{2+}$ binding of the high affinity indicator. Finally, we constructed a translocating $Ca^{2+}$ sensor, consisting of the $Ca^{2+}$-sensing protein kinase C α C-terminally fused to the red fluorescent protein mCherry2 (PKCα$_{mCherry2}$; $\lambda_{ex}$ = 589 nm, $\lambda_{em}$ = 610 nm; Fig. 3E, F). Since plasma membrane translocation of PKCα$_{mCherry2}$ increases the amount of fluorescent proteins in the TIRF volume, the fusion protein can be regarded as a $Ca^{2+}$ indicator in TIRF microscopy. Indeed, PKCα$_{mCherry2}$ reliably reported every single $Ca^{2+}$ spike that was identified by Cal520ff in the same cell (Fig. 3F). Therefore, PKCα$_{mCherry2}$ was chosen as red $Ca^{2+}$indicator for further experiments. The mechanism of $Ca^{2+}$dependent membrane accumulation of PKCα might cause a slight time offset between the Cal520ff signal upstrokes and those of PKCα$_{mCherry2}$. To quantify this delay, we imaged glucose-induced $Ca^{2+}$ spikes in PKCα$_{mCherry2}$-expressing Cal520ff-loaded INS-1 cells by TIRF microscopy with a frame rate of 250 Hz. Analysis of consecutive spikes of Cal520ff and PKCα$_{mCherry2}$ signals yielded a temporal difference between time points of half-maximal upstroke of 3.6 ± 4.1 ms (n = 9;

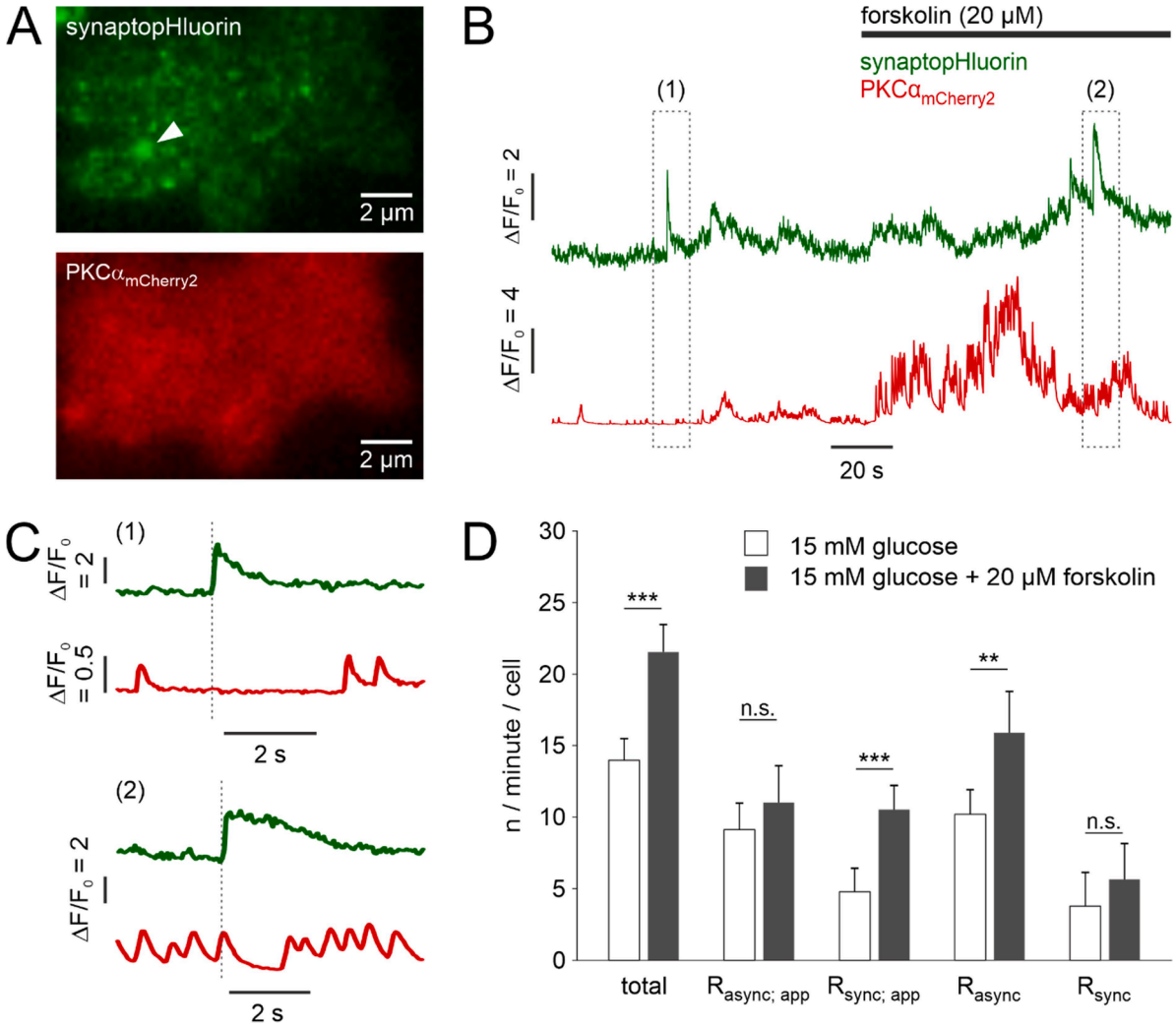


**Fig. 4.** Forskolin significantly increases the rate of vesicle fusions without increasing the synchronized fraction. **(A)** Raw data images show an INS-1 cell expressing synapthopHluorin (green) and PKCα$_{mCherry2}$ (red). **(B)** Time course of fluorescence changes in the INS-1 cell depicted in **(A)**. The red PKCα$_{mCherry2}$ graph represents the fluorescence changes averaged over the whole cell. The green synaptopHluorin graph corresponds to the region marked in **(A)** (arrowhead). The black bar represents the addition of forskolin (20 µM). **(C)** Fluorescence changes of the signals framed and numbered in **(B)** are shown in a higher temporal resolution. **(D)** Statistical analysis of total, apparent asynchronous ($R_{async; app}$), apparent synchronous ($R_{sync; app}$), asynchronous ($R_{async}$) and synchronous ($R_{sync}$) fusions $min^{-1}$ $cell^{-1}$ before and after the addition of forskolin (20 µM) ($n$ = 10 cells. Statistical analysis was performed using the Wilcoxon signed-rank test for non-parametric paired data, *$p \leq 0.05$, **$p \leq 0.01$, ***$p \leq 0.005$, bars: means and S.E.). The correlation refers to a $Ca^{2+}$ upstroke within 500 ms relative to each fusion. For the calculation of $R_{async}$ and $R_{sync}$ see main text.

Fig. 3G, H), which was considered sufficiently low to accept PKCα$_{mCherry2}$ as a fast responding $Ca^{2+}$ biosensor. Due to the ongoing accumulation within the plasma membrane and the higher $Ca^{2+}$ binding affinity of PKCα, the peak PKCα$_{mCherry2}$ signals were reached with a longer delay of approximately 40–60 ms, and the off rates were slower than those of Cal520ff-reported signals.

### 2.3. Co-imaging of $Ca^{2+}$ spikes and fusion events

Simultaneous dual-color TIRF microscopy of INS-1 cells co-expressing synaptopHluorin and PKCα$_{mCherry2}$ (Fig. 4 A, B) revealed vesicles fusing at time points between $Ca^{2+}$ spikes as well as fusions during or shortly after a preceding $Ca^{2+}$ spike (Fig. 4C). An empirically defined time interval for temporal correlation was set to 500 ms, starting 100 ms before the $Ca^{2+}$upstroke and ending 400 ms after the signal. During glucose-induced $Ca^{2+}$ spiking, 65 % of all fusion events occurred outside this defined interval and, therefore, appeared to represent a non-synchronized fraction $F_{asynch;\ app}$ with respect to $Ca^{2+}$upstroke events (Fig. 4D). The remaining fraction (35 % of fusion events) appeared synchronized ($F_{sync;\ app}$), although some fusions would only coincidentally happen within the arbitrarily defined 500 ms interval, without being triggered by the corresponding $Ca^{2+}$ spike. To correct for such coincidence and obtain an estimate for true fractions of synchronized versus asynchronous fusion events $F_{synch}$ and $F_{asynch}$, a binary $Ca^{2+}$ trace was generated with high $[Ca^{2+}]_i$ defined within the 500-ms interval around the $Ca^{2+}$ upstroke, and all appearing fusions were plotted against it (Suppl. Fig. S3). Assuming that the rate of asynchronous fusion events during phases of high $[Ca^{2+}]_i$ is the same as for phases of low $[Ca^{2+}]_i$, $F_{asynch}$ would calculate as:

$$F_{asynch} = F_{asynch;app} \frac{total\ observation\ time}{observation\ time\ with\ low\ [Ca^{2+}]_i} \quad (1)$$

Then, the fraction of estimated true synchronized events would be $F_{synch} = 1 - F_{asynch}$. The corresponding rates of estimated true synchronized and asynchrounous release events per cell $R_{synch}$ and $R_{asynch}$ are then obtained by determining the total fusion rates $R_{total}$ multiplied by the respective fractions. After applying this correction, the estimate for $R_{synch}$ in glucose (15 mM)-stimulated INS-1 cells dropped about 22 % compared to $R_{synch;app}$. Upon additional stimulation with forskolin, $R_{asynch}$ increased about 56 %, whereas $R_{synch}$ was only trending to increase, without reaching a statistically significant difference (Fig. 4D). Of note, the fraction of synchronized fusion events $F_{synch}$ did not increase upon forskolin stimulation. Similar results were obtained after exposing INS-1 cells to the sulfonylurea receptor agonist tolbutamide (Suppl. Fig. S4).

### 2.4. Simulation of $Ca^{2+}$uncorrelated and $Ca^{2+}$triggered fusion events

The estimates outlined above still rely on the binarization of $Ca^{2+}$ traces into phases of low and high $[Ca^{2+}]_i$. To assess the rates and fractions of synchronized versus asynchronous release events with a complementary method, we reasoned that in case of synchronization, a temporally correlated $Ca^{2+}$ signal upstroke should precede, but not follow a fusion event. In contrast, an asynchronous release would show no such preference, and the temporally closest $Ca^{2+}$ signal upstrokes would symmetrically distribute before and after the fusion event. The frame number $X$ is a discrete random variable with $X_{fusion}$ describing the frame number in which the fusion event was first detected. In case of asynchronous release, the probability distribution of the temporally closest $Ca^{2+}$upstroke $p_{Ca2+upstroke;\ asynch}(X)$ appearing in a frame taken before or after a fusion event occurring at $X_{fusion}$ can be described as

$$p_{Ca^{2+}\ upstroke,asynch}(X) = 0.5\ p_{Ca^{2+}\ upstroke} * \left(1 - p_{Ca^{2+}upstroke}\right)^{|X - X_{fusion}|} \quad (2)$$

with $p_{Ca2+upstroke}$ representing the probability of observing a $Ca^{2+}$ upstroke in a random frame. In continuous imaging with no interspersed dark times, the resulting set of modeled curves shows the expected symmetric temporal pattern around the time point of vesicle fusions (Fig. 5A). In contrast, the probability distribution of $Ca^{2+}$upstrokes that induce a synchronized fusion event would follow an asymmetric pattern with a Poisson distribution of the frame count showing the temporally closest $Ca^{2+}$ upstroke, which precedes the fusion event by an average frame number λ (Fig. 5B, left panel). The probability distribution would therefore calculate for each imaging frame number $X$ as

$$p_{Ca^{2+}\ upstroke;\ synch}(X) = \frac{\lambda^{X_{fusion} - X}}{(X_{fusion} - X)!} e^{-\lambda} \quad (3)$$

In case of delayed reporting of $Ca^{2+}$ upstrokes by the used indicator, the probability function may be horizontally shifted by a small amount, according to the time offset between the actual $Ca^{2+}$influx and the upstroke of the PKCα$_{mCherry2}$ signal (inset in Fig. 5B).

To simulate a scenario of mostly asynchronous release, the equations (2) and (3) were multiplied by the number of fusions following the respective patterns, and summed up. Binned to 50-ms time intervals, corresponding to the experimentally applied frame rate of 20 Hz, a histogram of 2000 fusion events of which 90 % were asynchronous yielded a pattern as depicted in Fig. 5C. An acquisition frequency of 20 Hz, an average $Ca^{2+}$upstroke frequency of 2 Hz, an expected median delay between $Ca^{2+}$ upstroke and synchronized fusion events of $\lambda = 32$ ms and a time difference of 4 ms between the actual $Ca^{2+}$influx and its reporting by the upstroke of the PKCα$_{mCherry2}$ fluorescence signal was chosen to match the experimental conditions. In the next step, the mathematical model was fitted to the experimental data.

### 2.5. Synchronized and asynchronous fusion events in glucose-exposed INS-1 cells before and after stimulation with forskolin or tolbutamide

$Ca^{2+}$spiking in INS-1 cells was initiated in KRHB, containing 5 mM or 15 mM glucose, and further stimulated by forskolin (20 μM) or tolbutamide (50 μM) during simultaneous TIRF imaging of synaptopHluorin and PKCα$_{mCherry2}$ fluorescence. The temporally closest $Ca^{2+}$upstroke events ($\Delta t \leq 1$ s) were plotted in a histogram (Fig. 6A, B), containing information of 164 fusions events before and 1190 events after stimulation of the same cells. Notably, a substantial number of fusion events was not accompanied by $Ca^{2+}$ spikes within a 1-s window ($\Delta t > 1$ s in Fig. 6A, B). In all other cases, a major fraction of temporally closest $Ca^{2+}$ upstroke events ($\Delta t \leq 1$ s) was distributed symmetrically around the fusion event, but a remaining asymmetry of the histogram was evident before as well as after treatment of the cells (Fig. 6B), indicating that a fraction of fusions is synchronized with a preceding $Ca^{2+}$upstroke. The rate of synchronized fusions was quantified by applying a global fit of the sum of the probability functions for synchronized and asynchronous release multiplied by the total rate of fusion events to the experimental data (Fig. 6C, D). After forskolin or tolbutamide treatment, 1.6 fusions $min^{-1}$ $cell^{-1}$ were synchronized with $Ca^{2+}$spikes, compared to 0.61 fusions $min^{-1}$ $cell^{-1}$ before stimulation. The percentage of synchronized fusions of all fusion events slightly increased from 5.3 % before to 7.2 % after treatment. Apparently, only a fraction of vesicle fusions appears in a synchronized, $Ca^{2+}$triggered manner. Supporting this notion, in INS-1 cells showing a low density of $Ca^{2+}$ channel activity, vesicle fusions occurred not only temporally but also spatially loosely coupled to the sites of $Ca^{2+}$ entry (Fig. 7). Although the sites of $Ca^{2+}$ influx were mostly located in cellular protrusions (Fig. 7A and Suppl. Fig. S2), vesicle fusions occurred mostly in the center of the cell and up to 20 μm distant from regions that are engaged in $Ca^{2+}$ spiking (Fig. 7B). Since a scaffolding of voltage-gated $Ca^{2+}$ channels around focal adhesion kinase and ELKS has been proposed [27], we assessed the organisation of focal adhesions in INS-1 cells by imaging the subcellular distribution of heterologously expressed vinculin$_{RFP}$ and F-tractin$_{GFP}$ (Suppl. Fig. S5–8). INS-1 cells showed a canonical organization of vinculin spikes on poly-L-lysine- or on laminin-coated coverslips, providing anchorage sites for

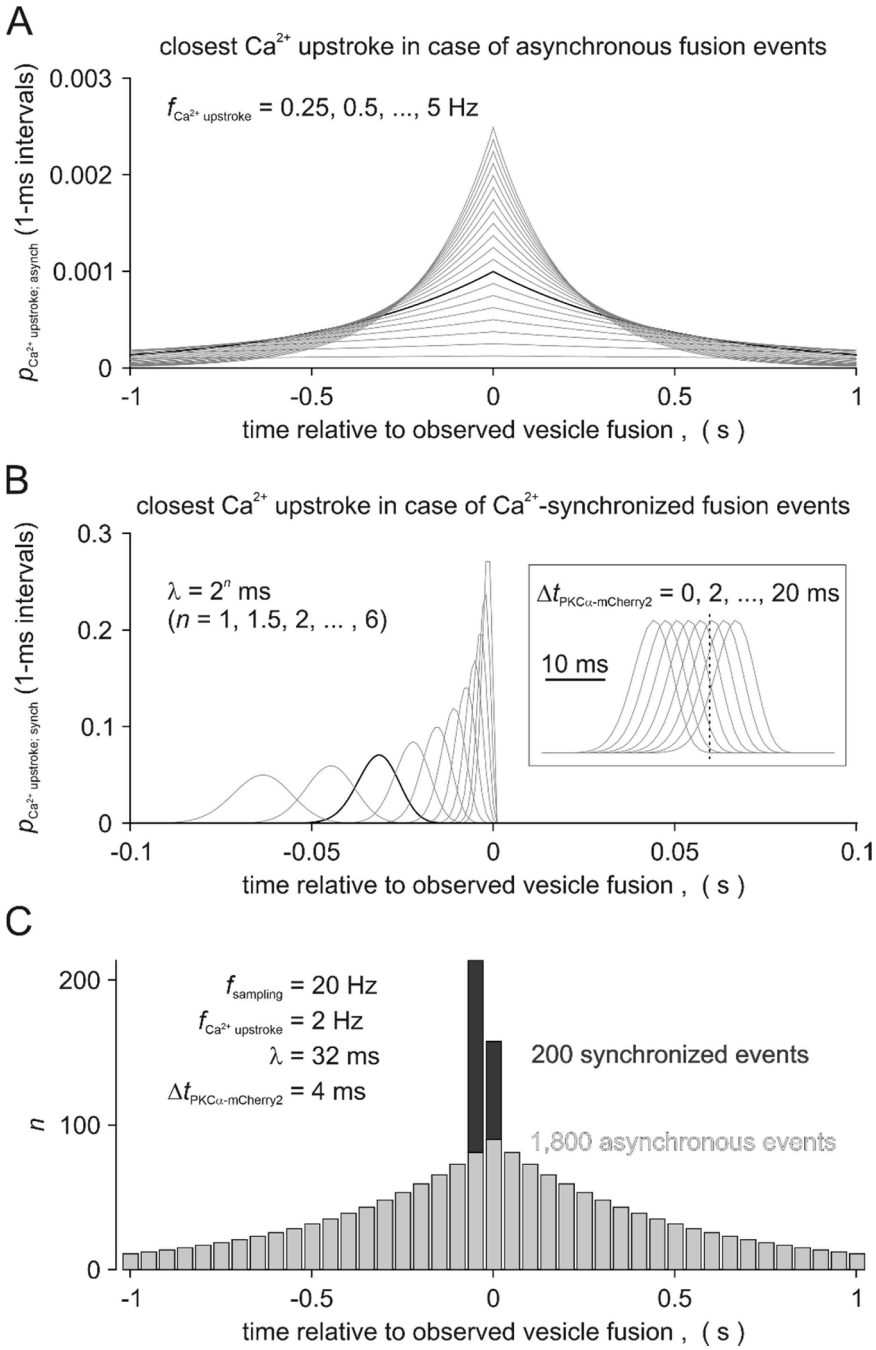


**Fig. 5.** Simulation of distinct temporal patterns caused by $Ca^{2+}$-uncorrelated or $Ca^{2+}$-triggered fusion events. **(A)** Probability distribution of temporally closest subplasmalemmal $Ca^{2+}$ upstrokes appearing before or after a vesicle fusion in case of $Ca^{2+}$-independent vesicle fusion events. Note the symmetry of the probability function at any frequency of $Ca^{2+}$ spiking. Data are calculated for 50 ms-bins, corresponding to the image acquisition frequency applied in experimental settings. **(B)** Poisson distribution of closest $Ca^{2+}$ upstrokes preceding the vesicle fusion by the expected times λ (left panel) and impact of 0–20 ms delay of $PKC\alpha_{mCherry2}$ reporting the $Ca^{2+}$ upstroke (right panel). **(C)** Synthetic data exemplifying a scenario with 10 % exocytotic events triggered by subplasmalemmal $Ca^{2+}$ spikes and 90 % fusion events triggered independently of individual subplamalemmal $Ca^{2+}$ spikes.

actin filaments in cellular protrusions (Suppl. Fig. S5, S6). Thus, the preference of $Ca^{2+}$ influx sites in such protrusions (Suppl. Fig. S7) may rely on the proposed local clustering of voltage-gated $Ca^{2+}$ channels. Nonetheless, we could not observe a local preference for fusion events in the vicinity of focal adhesions (Suppl. Fig. S8), thereby corroborating the finding of spatially loose coupling between $Ca^{2+}$ influx and fusion events.

## 3. Discussion

In this study, we have developed a methodological framework to simultaneously monitor subplasmalemmal increases in $Ca^{2+}$ and exocytotic events at a spatial and temporal resolution, which allows for a discrimination between synchronous and asynchronous coupling between $Ca^{2+}$ spikes and release of insulin-containing granules. The major and unexpected finding was that despite demonstration of short-lived and sometimes spatially restricted subplasmalemmal $Ca^{2+}$ signals, reaching peak concentrations of 2–5 μM [14], a large fraction of

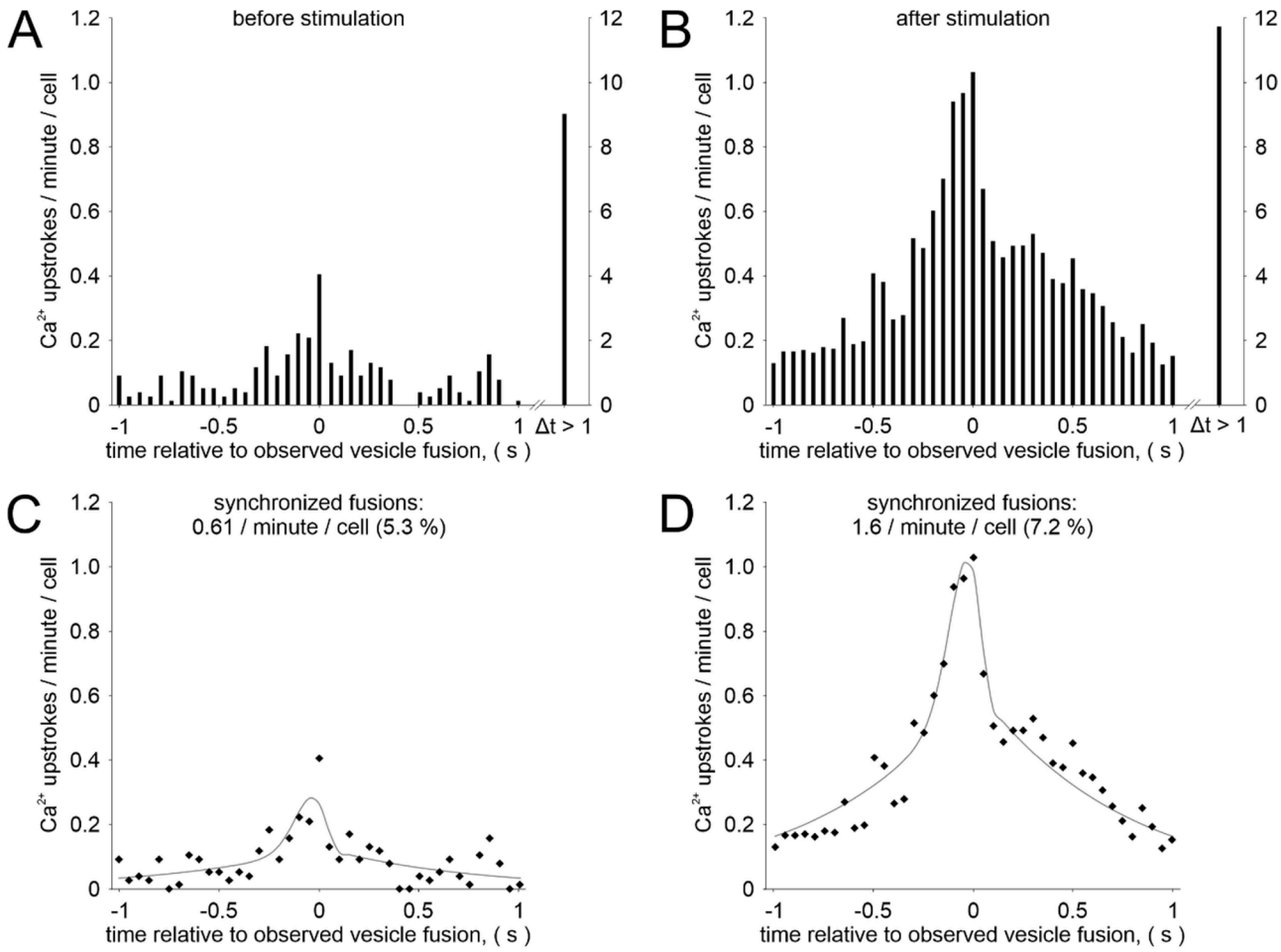


**Fig. 6.** The amount of fusions correlated to a subplasmalemmal $Ca^{2+}$ upstroke increases slightly after stimulation with forskolin or tolbutamide. **(A, B)** Histogram representation of the temporal distance of the closest $Ca^{2+}$ upstroke preceding (< 0 s), coinciding with (0 s), or following (> 0 s) individual fusion events in the respective observed cell. Note that fusion events occurring outside a 1-s-interval before or after fusion ($\Delta t > 1$) are drawn at a different scale. Data are aggregated for 46 cells observed in $n = 34$ independent experiments. Shown are histograms obtained from data of the same INS-1 cells before **(A)** or after **(B)** exposure to forskolin (20 μM) or tolbutamide (50 μM). **(C, D)** Analysis of the contribution of asynchronous and synchronized fusion events to the data shown in **(A, B)**, according to their expected symmetric or asymmetric temporal patterns as shown in Fig. 5. For details of the fitting procedure, refer to the main text. INS-1 cells were kept in KRHB solution supplemented with either 5 or 15 mM glucose.

exocytotic events in either resting or stimulated INS-1 cells was not synchronized with the $Ca^{2+}$ spiking. The trains of $Ca^{2+}$ spikes are presumably reflecting opening of voltage-gated $Ca^{2+}$ channels, of which the L-type channels $Ca_V1.2$ and $Ca_V1.3$ are most abundant, although several other subtypes are also expressed in pancreatic beta cells as well as in INS-1 cells [28,29]. The observation of homogenous subplasmalemmal $Ca^{2+}$ spiking in most cells points to a channel density that exceeds the size of single $Ca^{2+}$ microdomains when monitored with a low affinity indicator dye at frequencies of 50–200 $s^{-1}$.

After narrowing down $Ca^{2+}$ microdomains in patched beta cells intracellularly perfused with high concentrations of the slowly binding $Ca^{2+}$ chelator EGTA while engaging $Ca_V$ channel opening by means of membrane depolarization, a spotty pattern of locally elevated subplasmalemmal $Ca^{2+}$ concentrations was detectable in TIRF microscopy [30]. Our experiments applying the cell-permeant EGTA-AM for intracellular loading with EGTA confirm these findings in freely oscillating INS-1 cells (Suppl. Fig. S2). In the absence of intracellularly loaded EGTA or BAPTA, rapid diffusion of free $Ca^{2+}$ with a reported diffusion coefficient of $D = 220$ $\mu m^2/s$, and of indicator-bound $Ca^{2+}$ (estimated $D = 100$–$120$ $\mu m^2/s$; [24]) presumably restricted the cases of observable microdomains to those cells in which only few and distantly located $Ca_V$ channels became activated. $Ca^{2+}$ signals became absent after loading the INS-1 cells with 30 μM EGTA-AM, however the fusion rate did not decrease significantly (Fig. 1). In line with reports on a focal adhesion kinase- and integrin-dependent recruitment of ELKS and local initiation of $Ca^{2+}$ signals in glucose-stimulated beta cells [27], we observed a preferential positioning of $Ca^{2+}$ entry sites close to the focal adhesions in these cells (Suppl. Fig. S7), which could be seen in cells cultured on laminin- as well as poly-L-lysine-coated coverslips (Suppl. Fig. S5, S6). Under such conditions, the half width of the spatially spreading microdomain is expected to rise above 1.5 μm within 2 ms as calculated in a computational model and shown experimentally (Fig. 2). Are these subplasmalemmal $Ca^{2+}$ fluctuations sufficient to acutely trigger exocytosis of granules within an active zone-like $Ca^{2+}$ microdomain? A number of active zone proteins, such as Munc13–1, RIM2, Piccolo, Bassoon, and ELKS are expressed in beta cells ([16] and references therein) may physically link primed vesicles to voltage-gated $Ca^{2+}$ channels and SNAP-25/Syntaxin1. In addition, medium- to high-affinity synaptotagmins, such as Syt7 have been proposed as $Ca^{2+}$ sensors for insulin release from beta cells [31], and may become activated within subplasmalemmal $Ca^{2+}$ microdomains. Indeed, findings obtained with electrophysiological methods have demonstrated that a fraction of exocytotic events can be acutely triggered by rectangular depolarising pulses applied at a duration of 30 ms or longer as measured by immediate increases in cell capacitance [13,32].

Since electrophysiological capacitance measurements are obtained

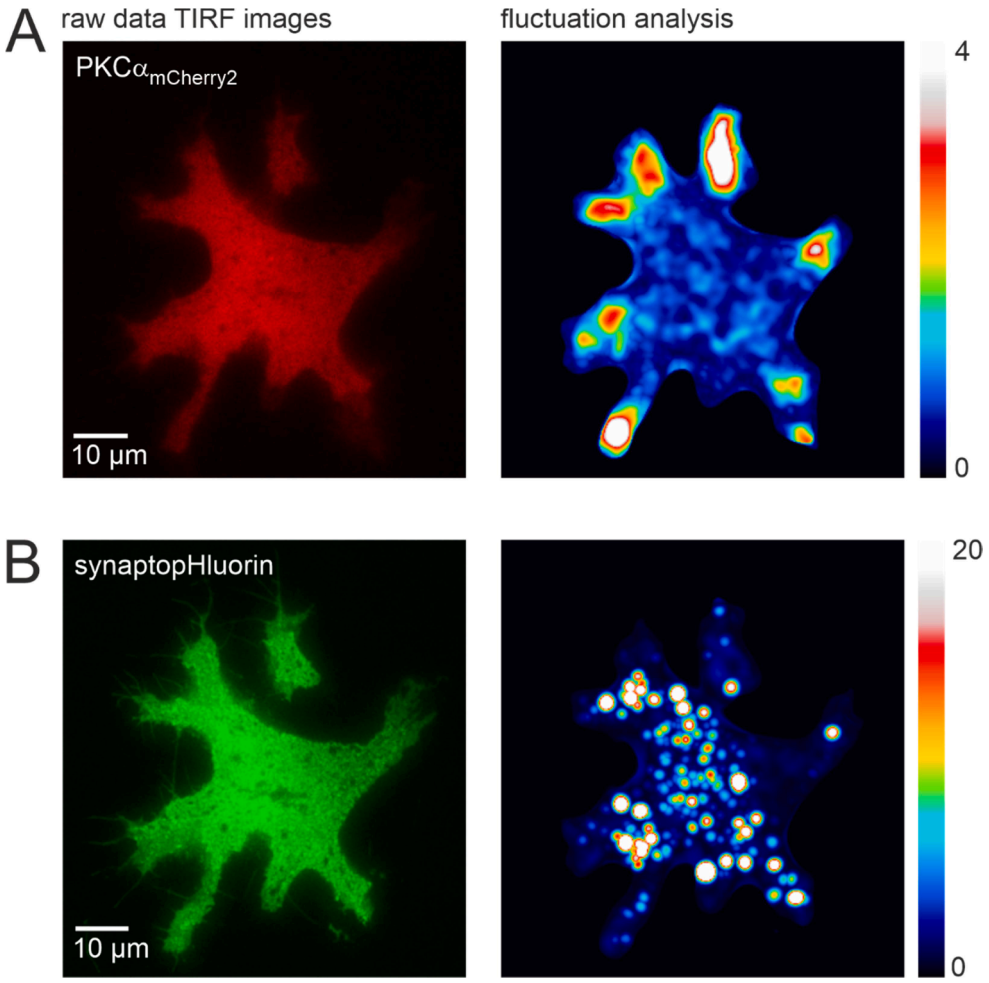


**Fig. 7.** Vesicles fuse spatially loosely coupled to $Ca^{2+}$signals. TIRF microscopy of $Ca^{2+}$ signals **(A)** and synaptopHluorin signals **(B)** in an INS-1 cell showing localized, but synchronized $Ca^{2+}$ fluctuations. PKC$\alpha_{mCherry2}$ (red) and synapthopHluorin (green) were simultaneously imaged at 20 Hz (left panels), and data were subjected to a variance analysis to visualize the localization of $Ca^{2+}$ entry and fusion events (right panels). INS-1 cells were kept in KRHB solution supplemented with 5 mM glucose, and stimulated with tolbutamide (50 μM). The variance was calculated over consecutive bins comprising 10 frames, each, and divided by the mean fluorescence. To visualize the fusion sites, the maxima of 400 bins were superimposed.

in the whole cell configuration, the intracellular concentrations of ions, $Ca^{2+}$ buffers, ATP and other solutes are tightly controlled by the pipette solution, the membrane potential or transmembrane currents are clamped, and stimuli can be applied in a precisely timed fashion. Our measurements complement these data by allowing membrane potentials, currents and intracellular ion concentrations to freely fluctuate with minor impact on intracellular signalling cascades. As outlined in Fig. 2, the rising phase of $Ca^{2+}$ spikes is shorter than 30 ms, which is in line with the reported duration of single action potentials that typically show a half-width shorter than 20 ms [33]. Thus, single action potential-driven $Ca^{2+}$ spikes may not reach the required peak concentrations and/or duration for efficient secretion coupling in INS-1 cells. Amperometric detection methods allow the recording of single exocytotic events in pancreatic beta cells by directly measuring the oxidation of insulin [34,35] or, after pre-loading cells with serotonin, by electroconversion of serotonin as a surrogate marker for co-released insulin [36]. Although amperometric methods bear the potential to record single secretory events, recordings with simultaneous, spatiotemporally resolved imaging of subplasmalemmal $Ca^{2+}$ fluctuations are not available. Therefore, these data provide limited information about the immediate coupling between $Ca^{2+}$ channel openings and insulin granule release. In mouse pancreatic beta cells as well as in INS-1 cells, photolysis of intracellularly loaded caged $Ca^{2+}$ does induce an immediate, but small rise in cell capacitance, followed by a slow, but larger second phase [10,37]. Similar observations have been made in patched human beta cells activated after applying 500-ms depolarising pulses [38]. In another set of experiments, fast exocytosis has been shown to require a $Ca^{2+}$ concentration of more than 8 μM, and half maximally efficient concentrations were about 17 μM [13], which is markedly higher than subplasmalemmal peak $Ca^{2+}$ concentrations detected in INS-1 cells in this study. These and other findings clearly demonstrate the existence of an RRP of insulin granules in beta cells that can be quickly released upon application of strong physiological or supra-physiological stimuli.

Glucose homeostasis critically relies on a finely tuned insulin secretion in response to elevated glucose levels, incretin signalling or upon application of antidiabetic drugs. Since beta cells in single murine islets are electrically coupled via gap junctions and display highly synchronized $Ca^{2+}$ influx signals upon exposure to elevated glucose concentrations [39,40], a tight physical coupling and synchronized release of a large fraction of insulin-containing granules would not fulfil this regulatory requirement. There are two general scenarios that could explain how graded responses can be achieved: one would be that between individual $Ca^{2+}$ spikes, a small RRP is replenished in a regulated fashion, leading to a limited size of this pool; alternatively, a second pool of granules would coexist, and be released in a temporally uncorrelated fashion. In the first case, we would expect that $Ca^{2+}$ spikes and exocytotic events would often or increasingly coincide upon stimulation,

which was, however, not the case. In fact, we observed an absolute increase in correlated fusion event rates from 0.61 fusions $min^{-1}$ $cell^{-1}$ before stimulation to 1.6 fusions $min^{-1}$ $cell^{-1}$ after stimulation (Fig. 5), but the percentage of synchronized fusions only slightly increased from 5.3 % to 7.2 %. After increasing the frequency of subplasmalemmal $[Ca^{2+}]_i$ spiking by glucose stimulation, the amount of asynchronous exocytosis events rose more strongly than that of synchronized fusions. Supporting this notion, we observed several fusion events occurring without $Ca^{2+}$ spiking in the corresponding region of the cell (Suppl. Fig. S3). Thus, our initial expectation that most exocytotic events would be acutely triggered by single subplasmalemmal $Ca^{2+}$ spikes detected in TIRF microscopy was not confirmed. Instead, we were surprised to see that, although such events do exist, the majority of release events in INS-1 cells either happen in phases with lower subplasmalemmal $Ca^{2+}$ concentrations or only coincidentally overlap with a $Ca^{2+}$ spike, especially after strongly increasing the $Ca^{2+}$ spike frequency by stimulation with glucose, tolbutamide or forskolin. Both, the spatial spread of subplasmalemmal $Ca^{2+}$ signals and the large amount of asynchronous granule release from INS-1 cells closely resemble the loose temporal coupling between $Ca^{2+}$ channel activity and exocytosis that has been described in chromaffin cells [21].

If only a minority of granules is contained in and released from an RRP, what are then candidate mechanisms of loose coupling? The temporal dissociation between single $Ca^{2+}$ spikes and fusion events points to a critical role of more long-lived signalling pathways. One major discrimination is between $K_{ATP}$ channel-dependent and $K_{ATP}$ channel-independent signalling cascades. The latter include the incretin-mediated and cAMP-dependent stimulation of exchange protein directly activated by cAMP (EPAC) 2A and of protein kinase A, which enlarges the pool of vesicles that can be released in response to membrane depolarization or photolysis of caged $Ca^{2+}$ [41–43]. Another pathway acts through the activation of Gq-protein-coupled receptors, phospholipase C and PKC, which sensitizes $Na^+$channels to promote the depolarization and secondary $Ca^{2+}$ influx [10,44,45]. Because of the increased $[Ca^{2+}]_i$, CaMKII is activated, which has also been reported to accelerate vesicle mobility and the refilling of the RRP [46]. Diacylglycerols (DAG) formed either by Gq-activated phospholipase C β isoforms or via EPAC2A-Rap1-phospholipase C ε-mediated signalling [47] may serve to recruit Munc13–1 to the plasma membrane, where it interacts with Syntaxin1 and critically determines vesicle priming, thereby increasing the possibility of fusion [48–50]. Munc13-1 is critical for exocytosis in general as knock-out mice show almost no fusion events at all: While Munc13-1 knockout mice died shortly after birth, even heterozygous mice showed a decrease of 52 % in glucose-induced insulin secretion [49].

In line with our data there are several studies, showing that synaptotagmins, especially Syt7, which acts as a high affinity $Ca^{2+}$ sensor for exocytosis in pancreatic β-cells, does play an important role in fusion events, but knock-out mice show only a partial reduction of basal or glucose-induced insulin secretion. The basal insulin secretion in Syt7 depleted human islets was not different at all, whereas the first and second phase of glucose-induced insulin secretion was decreased by up to 39.5 %, matching the 40 % loss of glucose-induced insulin secretion in islets from Syt7 knockout mice [51–53]. We, therefore, propose a model in which insulin release in part relies on acute $Ca^{2+}$ influx-triggered fusion events, and another fraction that is exocytosed without a tight synchronisation to $Ca^{2+}$ influx events, but in a temporally and spatially loosely coupled fashion. Of note, high affinity synaptotagmins such as Syt7 may contribute to asynchronous release as well, as shown in hippocampal neurons [54].

There are numerous caveats that should not be neglected before generalizing our findings to mechanisms of insulin release in vivo. Most obviously, rat INS-1 cells are a model for, but not identical to native beta cells in rodents and even less so for human beta cells. Although their repertoire of voltage-gated $Ca^{2+}$ channels closely matches that of native rat pancreatic beta cells [29], channel densities, expression of auxiliary $Ca^{2+}$ channel subunits, but also the expression and function of other channels that constitute the electrical oscillator and regulate the driving force for $Ca^{2+}$ entry through $Ca_V$ channels may differ from the native situation. For example, localized clusters of non-randomly distributed $Ca_V$ channels as demonstrated by Hoppa et al. [30] may shape $Ca^{2+}$ "super-microdomains" reaching substantially higher central peak concentrations and more efficiently engage medium- to high-affinity $Ca^{2+}$ sensors than subplasmalemmal microdomains demonstrated in this study.

In the context of native beta cells, polarized secretion towards the capillary interface has been demonstrated, and local clustering of active zone-like proteins at focal adhesions likely contributes to this effect [16, 27]. In cultured INS-1 cells, focal adhesions are present and canonically organized (Suppl. Fig. S5, S6), indicating an intact integrin signalling, and synthesis of matrix proteins, such as laminins. Although $Ca_V$ channels appeared to reside close to such focal adhesions (Suppl. Fig. S7), we did not observe a local accumulation of fusion events in these regions (Suppl. Fig. S8). Thus, the 3D architecture, paracrine communication with capillary endothelial cells, or simply a lack of one or several proteins may render INS-1 cells defective for efficient synchronization and proper subcellular targeting of exocytosis. On the other hand, INS-1 cells do feature a readily releasable pool, which can be engaged by stimulatory regimes that are also effective in native beta cells. In addition, considering that TIRF microscopy selectively integrates fusion events occurring at the bottom of the cells with an average area of 384 $\mu m^2 \pm$ 38.7 $\mu m^2$ (mean and S.E. of 46 imaged cells), the observed secretion rates in INS-1 cells of 13.97 fusions $min^{-1}$ $cell^{-1}$ before and 21.55 fusions $min^{-1}$ $cell^{-1}$ after forskolin treatment match the reported exocytotic performance of INS-1 and even native β-cells [53,55]. Finally, despite demonstration of the spatial overlap of $Ca^{2+}$ signalling and release sites in native beta cells, a temporal synchronization of insulin secretion with individual spikes of glucose-induced and $Ca_V$-mediated influx events has not yet been investigated in intact islets or in organotypic tissue slice cultures.

Although we have been using a $Ca^{2+}$ indicator dye with a very low $Ca^{2+}$-binding affinity of 10 μM, a local buffering effect, as well as an increased lateral mobility of indicator-associated calcium ions cannot be excluded. In simultaneous co-imaging experiments of $Ca^{2+}$ fluctuations and exocytosis events, however, no low molecular weight $Ca^{2+}$ indicator was loaded. Instead, we were relying on the diffusion-driven and diffusion-delimited membrane association of a heterologously expressed autofluorescent PKC α fusion protein [56]. This strategy presumably avoids the increased mobility of $Ca^{2+}$, but may impose other problems, such as a slight delay of response to channel openings, which we have characterized and compensated for by introducing a delay term in the global fit algorithm. The overexpressed PKC itself may also interfere with signalling pathways. Activation of PKC, however, additionally requires diacylglycerols to dissociate the intramolecular pseudosubstrate from the active center. A delay in the release of insulin or insulin hexamers has been reported and attributed to a delayed expansion of the fusion pore and the large size of the cargo [57]. Since we were detecting fusion events by monitoring the rise of the luminal pH rather than by monitoring the exit of large cargo through a slowly expanding fusion pore, our co-imaging method is unlikely to be distorted by such delay. Finally, the TIRF microscopy yields an exceptionally good signal-to-noise ratio in detecting processes within or close to the plasma membrane, but it intrinsically blinds us to processes happening in other compartments, including the plasma membrane in the upper part of the cell or at cell-to-cell contacts.

Taken together, we provide evidence for the coexistence of $Ca^{2+}$-triggered synchronized fusion events, and asynchronous granule release from INS-1 cells. The latter accounts for the majority of exocytotic events in both resting and in glucose-stimulated cells. High-speed TIRF microscopy of differently labeled genetically encoded fast-responding biosensors allows the simultaneous imaging of subplasmalemmal $Ca^{2+}$ fluctuations and thereby provides a simple means to investigate

temporal and spatial patterns of stimulus-secretion coupling in otherwise undisturbed cells. Further studies are needed to assess how $Ca^{2+}$ signals are coupled to insulin release from murine and human beta cells.

## 4. Materials and methods

### 4.1. Reagents

Unless otherwise stated, all chemicals were purchased from Merck KgaA (Darmstadt, Germany).

### 4.2. Cell culture

Rat insulinoma INS-1 cells were cultivated in RPMI1640 culture medium containing 11.1 mM glucose and supplemented with 10 % fetal calf serum (ThermoFisher, Waltham, USA), 100 Units/ml penicillin, 0.1 mg/ml streptomycin, 0.2 mM L-glutamine, 50 μM 2-mercaptoethanol, 10 mM 2-hydroxyethylpiperazin-N′−2-ethansulfonsäure (HEPES, Carl Roth, Karlsruhe, Germany) and 1 mM sodium pyruvate. Cells were maintained in a humidified atmosphere at 37 °C and 5 % $CO_2$.

### 4.3. Molecular biology

The coding sequence of mCherry2 was subcloned into the XbaI/ApaI sites of a pcDNA3 vector to obtain a pcDNA3-mCherry2 plasmid. The open reading frame of human PKCα lacking a stop codon was cut out of a pcDNA3-PKCα-YFP vector using HindIII and XhoI (both New England Biolabs GmbH).

### 4.4. Total internal reflection fluorescence (TIRF) microscopy

A dual-color TIRF microscopy setup (Suppl. Fig. S9) was built around an inverted motorized Axio Z1 microscope (Carl Zeiss, Jena, Germany) essentially as described [58,59], but with a Spectra III light engine (Lumencor, Beaverton, USA) equipped with a 3 mm liquid light guide (LLG) as light source. The exit of the LLG was collimated with an aspherical lens (L1, f = 17.5 mm) and projected by means of an achromatic lens (L2, f = 80 mm) onto a pH 1/0.4 phase contrast microscopy annular aperture mask ($r_{inner}$ = 5.37 mm, $r_{outer}$ = 6.47 mm) in a 4.6-fold magnification. The image of the annular aperture was projected into the back focal plane of an α-Plan-Apochromat 63x/1.46 objective (Carl Zeiss, Jena Germany) by two achromatic lenses (L3a, f = 150 mm / L3b, f = 250 mm) that collimate the light and one plano-convex lens (L4, f = 125 mm) that matches the transversal chromatic aberration of Zeiss. By varying the distance between L3a and L3b, the projection size of the annular aperture could be changed. An adjustable field stop (1–15 mm diameter) was placed between L3b and L4 in a conjugated plane to the focal plane. The lenses and annular aperture were mounted onto an optical rail system (FLR40, Qioptiq, Göttingen, Germany) and placed on top of a motorized Micromanipulator 5171 stage (Eppendorf, Hamburg, Germany). The two excitation wavelengths (475 nm and 575 nm) were reflected into the objective by a dual band dichroic beamsplitter (Semrock, Rochester, USA). Emitted light of the probe was transmitted. Fluorescence emission was recorded with a low-noise cooled Hamamatsu Orca Quest camera (Hamamatsu Photonics, Hamamatsu, Japan) connected to an Optosplit II (Cairn, Faversham, UK) and a 0.63x phototube. The emitted light of the green and red fluorophores was filtered by 525/50 nm and 632/60 nm band pass filters respectively. Image acquisition was controlled by the MicroManager 2.0 gamma software. All lenses were purchased from Edmund Optics (Mainz, Germany).

### 4.5. Transient transfection

INS-1 cells were seeded onto poly-L-lysine coated 25 mm glass coverslips (neoLab, Heidelberg, Germany) or on coverslips coated overnight at 4 °C with 5 μg/ml Biolaminin 511 (Biolamina, Sundbyberg, Sweden), and transfected with 4 μl Lipofectamine 2000 (ThermoFisher) and 2 μg of cDNA plasmids, encoding CAR-GECO1 (Addgene, Watertown, USA), $PKC\alpha_{mCherry2}$, synaptobrevin-$2_{GFP}$ (synaptopHluorin [60]), $vinculin_{RFP}$ (Addgene, Watertown, USA), or F-$tractin_{GFP}$ (Addgene, Watertown, USA). For co-transfections, $PKC\alpha_{mCherry2}$- and synaptopHluorin-encoding plasmids were mixed in a 3:1 (1.5:0.5 μg) ratio. Imaging was performed 24–48 h after transfection.

### 4.6. Fluorescence imaging

INS-1 cells seeded onto poly-L-lysine-coated glass coverslips were incubated in RPMI 1640 culture medium supplemented with 2.5 mM probenecid (MedChemExpress LLC, Monmouth Junction, USA) and 500 nM X-Rhod-1-AM (ThermoFisher) and/or 10 μM Cal520ff-AM (Biomol, Hamburg, Deutschland). In imaging experiments applying intracellular $Ca^{2+}$ buffers, 10–30 μM EGTA-AM or 30 μM BAPTA-AM (both Th. Geyer, Renningen, Germany) were loaded at 37 °C for 30 min. After incubation, INS-1 cells were washed with Krebs-Ringer-Henseleit-buffer (KRHB), containing 136 mM NaCl, 4.7 mM KCl, 1.2 mM $MgSO_4$, 1.2 mM $KH_2PO_4$, 2 mM $NaHCO_3$, 10 mM HEPES (all chemicals from Carl Roth), 2 mM $CaCl_2$, 0.2 % bovine serum albumin and either 15 mM (high glucose KRHB) or 5 mM glucose (low glucose KRHB, Th. Geyer). For measurements performed in a $Ca^{2+}$-free buffer, we used nominally $Ca^{2+}$-free KRHB, supplemented with 0.5 mM EGTA. In some experiments, cells were pre-treated with 2 μM thapsigargin for 10–15 min to deplete thapsigargin-sensitive intracellular $Ca^{2+}$ stores.

During imaging experiments loaded or transfected INS-1 cells were maintained in KRHB at room temperature. For measurements under low glucose conditions, cells were incubated in KRHB containing 5 mM glucose at 37 °C for 30–60 min prior to imaging. To induce or accelerate $Ca^{2+}$ spikes in INS-1 cells, 20 μM forskolin or 50 μM tolbutamide in KRHB were added during the TIRF imaging. If not stated otherwise, an acquisition time of 50 ms (20 Hz), 2 × 2 binning and excitation wavelengths of 475 nm and 575 nm were used. Background signals were subtracted, and photobleaching was corrected, applying a bi-exponential fit. Data are presented as $F/F_0$.

### 4.7. Data and statistical analysis

Raw fluorescence data were analyzed with ImageJ software. Statistical analysis was performed using the Wilcoxon signed-rank test for non-parametric paired data or the *t*-test for parametric unpaired data. Normal distribution of the data was tested with the Kolmogorov-Smirnov test or the Wilcoxon-Mann-Whitney test for non-parametric unpaired data. Significance was accepted at $p < 0.05$.

## Funding

This work was supported by the Deutsche Forschungsgemeinschaft [TP18 in SFB-TRR 152].

## CRediT authorship contribution statement

**Charlotte Suckert:** Writing – original draft, Visualization, Investigation, Formal analysis. **Carolin Zosel:** Writing – original draft, Visualization, Investigation, Formal analysis. **Michael Schaefer:** Writing – original draft, Visualization, Supervision, Methodology, Conceptualization.

## Declaration of competing interest

The authors declare that they have no known competing financial interests or personal relationships that could have appeared to influence the work reported in this paper.

## Data availability

Data will be made available on request.

## Acknowledgments

We thank Gero Miesenböck for providing the expression plasmid encoding synaptopHluorin, and Marion Leonhardt and Nicole Urban for excellent technical assistance.

## Supplementary materials

Supplementary material associated with this article can be found, in the online version, at doi:10.1016/j.ceca.2024.102883.

## References

[1] P. Rorsman, F.M. Ashcroft, Pancreatic β-cell electrical activity and insulin secretion: of mice and men, Physiol. Rev. 98 (2018) 117–214, https://doi.org/10.1152/physrev.00008.2017.
[2] C. Ammälä, F.M. Ashcroft, P. Rorsman, Calcium-independent potentiation of insulin release by cyclic AMP in single beta-cells, Nature 363 (1993) 356–358, https://doi.org/10.1038/363356a0.
[3] A. Mayendraraj, M.M. Rosenkilde, L.S. Gasbjerg, GLP-1 and GIP receptor signaling in beta cells - A review of receptor interactions and co-stimulation, Peptides 151 (2022) 170749, https://doi.org/10.1016/j.peptides.2022.170749.
[4] A. Duttaroy, C.L. Zimliki, D. Gautam, Y. Cui, D. Mears, J. Wess, Muscarinic stimulation of pancreatic insulin and glucagon release is abolished in $M_3$ muscarinic acetylcholine receptor-deficient mice, Diabetes 53 (2004) 1714–1720, https://doi.org/10.2337/diabetes.53.7.1714.
[5] Z.L. Chu, R.M. Jones, H. He, C. Carroll, V. Gutierrez, A. Lucman, M. Moloney, H. Gao, H. Mondala, D. Bagnol, D. Unett, Y. Liang, K. Demarest, G. Semple, D. P. Behan, J. Leonard, A role for beta-cell-expressed G protein-coupled receptor 119 in glycemic control by enhancing glucose-dependent insulin release, Endocrinology 148 (2007) 2601–2609, https://doi.org/10.1210/en.2006-1608.
[6] D.A. Lang, D.R. Matthews, J. Peto, R.C. Turner, Cyclic oscillations of basal plasma glucose and insulin concentrations in human beings, N. Engl. J. Med. 301 (1979) 1023–1027, https://doi.org/10.1056/NEJM197911083011903.
[7] P. Gilon, R.M. Shepherd, J.C. Henquin, Oscillations of secretion driven by oscillations of cytoplasmic $Ca^{2+}$ as evidences in single pancreatic islets, J. Biol. Chem. 268 (1993) 22265–22268.
[8] M.C. Beauvois, C. Merezak, J.C. Jonas, M.A. Ravier, J.C. Henquin, P. Gilon, Glucose-induced mixed $[Ca^{2+}]_c$ oscillations in mouse β-cells are controlled by the membrane potential and the SERCA3 $Ca^{2+}$-ATPase of the endoplasmic reticulum, Am. J. Physiol. Cell Physiol. 290 (2006) C1503–C1511, https://doi.org/10.1152/ajpcell.00400.2005.
[9] T. Kanno, X. Ma, S. Barg, L. Eliasson, J. Galvanovskis, S. Göpel, M. Larsson, E. Renström, P. Rorsman, Large dense-core vesicle exocytosis in pancreatic beta-cells monitored by capacitance measurements, Methods 33 (2004) 302–311, https://doi.org/10.1016/j.ymeth.2004.01.003.
[10] Y. Yang, K.D. Gillis, A highly $Ca^{2+}$-sensitive pool of granules is regulated by glucose and protein kinases in insulin-secreting INS-1 cells, J. Gen. Physiol. 124 (2004) 641–651, https://doi.org/10.1085/jgp.200409081.
[11] B. Hastoy, M. Godazgar, A. Clark, V. Nylander, I. Spiliotis, M. van de Bunt, M. V. Chibalina, A. Barrett, C. Burrows, A.I. Tarasov, R. Scharfmann, A.L. Gloyn, P. Rorsman, Electrophysiological properties of human beta-cell lines EndoC-βH1 and -βH2 conform with human beta-cells, Sci. Rep. 8 (2018) 16994, https://doi.org/10.1038/s41598-018-34743-7.
[12] Z. Zhou, S. Misler, Amperometric detection of quantal secretion from patch-clamped rat pancreatic beta-cells, J. Biol. Chem. 271 (1996) 270–277, https://doi.org/10.1074/jbc.271.1.270.
[13] S. Barg, X. Ma, L. Eliasson, J. Galvanovskis, S.O. Göpel, S. Obermüller, J. Platzer, E. Renström, M. Trus, D. Atlas, J. Striessnig, P. Rorsman, Fast exocytosis with few $Ca^{2+}$ channels in insulin-secreting mouse pancreatic B cells, Biophys. J. 81 (2001) 3308–3323, https://doi.org/10.1016/S0006-3495(01)75964-4.
[14] G. Langlhofer, A. Kogel, M. Schaefer, Glucose-induced $[Ca^{2+}]_i$ oscillations in β cells are composed of trains of spikes within a subplasmalemmal microdomain, Cell Calcium 99 (2021) 102469, https://doi.org/10.1016/j.ceca.2021.102469.
[15] B.R. Gauthier, C.B. Wollheim, Synaptotagmins bind calcium to release insulin, Am. J. Physiol. Endocrinol. Metab. 295 (2008) E1279–E1286, https://doi.org/10.1152/ajpendo.90568.2008.
[16] M. Ohara-Imaizumi, K. Aoyagi, T. Ohtsuka, Role of the active zone protein, ELKS, in insulin secretion from pancreatic β-cells, Mol. Metab. 27S (2019) S81–S91, https://doi.org/10.1016/j.molmet.2019.06.017.
[17] K. Deng, P. Thorn, Presynaptic-like mechanisms and the control of insulin secretion in pancreatic β-cells, Cell Calcium 104 (2022) 102585, https://doi.org/10.1016/j.ceca.2022.102585.
[18] M.A. Fye, I. Kaverina, Insulin secretion hot spots in pancreatic β cells as secreting adhesions, Front. Cell Dev. Biol. 11 (2023) 1211482, https://doi.org/10.3389/fcell.2023.1211482.
[19] M. Hao, X. Li, M.A. Rizzo, J.V. Rocheleau, B.M. Dawant, D.W. Piston, Regulation of two insulin granule populations within the reserve pool by distinct calcium sources, J. Cell Sci. 118 (2005) 5873–5884, https://doi.org/10.1242/jcs.02684.
[20] G.G. Holz, O.G. Chepurny, C.A. Leech, W.J. Song, M. Hussain, Molecular basis of cAMP signaling in pancreatic beta cells, in: M.S. Islam (Ed.), Islets of Langerhans, 2. ed, Springer, Netherlands, Dordrecht, 2016, pp. 1–35.
[21] M.M. Wu, A. Llobet, L. Lagnado, Loose coupling between calcium channels and sites of exocytosis in chromaffin cells, J. Physiol. 587 (2009) 5377–5391, https://doi.org/10.1113/jphysiol.2009.176065.
[22] W.C. Tucker, E.R. Chapman, Role of synaptotagmin in Ca2+-triggered exocytosis, Biochem. J. 366 (2002) 1–13, https://doi.org/10.1042/BJ20020776.
[23] R. Yuste, R.B. Miller, K. Holthoff, S. Zhang, G. Miesenböck, Synapto-pHluorins: chimeras between pH-sensitive mutants of green fluorescent protein and synaptic vesicle membrane proteins as reporters of neurotransmitter release, Methods Enzymol. 327 (2000) 522–546, https://doi.org/10.1016/s0076-6879(00)27300-x.
[24] S.L. Mironov, Rethinking calcium profiles around single channels: the exponential and periodic calcium nanodomains, Sci. Rep. 9 (2019) 17196, https://doi.org/10.1038/s41598-019-53095-4.
[25] M. Oheim, M. van 't Hoff, A. Feltz, A. Zamaleeva, J.M. Mallet, M. Collot, New red-fluorescent calcium indicators for optogenetics, photoactivation and multi-color imaging, Biochim. Biophys. Acta 1843 (2014) 2284–2306, https://doi.org/10.1016/j.bbamcr.2014.03.010.
[26] J. Wu, L. Liu, T. Matsuda, Y. Zhao, A. Rebane, M. Drobizhev, Y.F. Chang, S. Araki, Y. Arai, K. March, T.E. Hughes, K. Sagou, T. Miyata, T. Nagai, W.H. Li, R. E. Campbell, Improved orange and red $Ca^{2+}$ indicators and photophysical considerations for optogenetic applications, ACS Chem. Neurosci. 4 (2013) 963–972, https://doi.org/10.1021/cn400012b.
[27] D. Jevon, K. Deng, N. Hallahan, K. Kumar, J. Tong, W.J. Gan, C. Tran, M. Bilek, P. Thorn, Local activation of focal adhesion kinase orchestrates the positioning of presynaptic scaffold proteins and Ca2+ signalling to control glucose-dependent insulin secretion, Elife 11 (2022), https://doi.org/10.7554/eLife.76262.
[28] M. Trus, R.F. Corkey, R. Nesher, A.-M.T. Richard, J.T. Deeney, B.E. Corkey, D. Atlas, The L-type voltage-gated $Ca^{2+}$ channel is the $Ca^{2+}$ sensor protein of stimulus-secretion coupling in pancreatic beta cells, Biochemistry 46 (2007) 14461–14467, https://doi.org/10.1021/bi7016816.
[29] S.N. Yang, P.O. Berggren, The role of voltage-gated calcium channels in pancreatic beta-cell physiology and pathophysiology, Endocr. Rev. 27 (2006) 621–676, https://doi.org/10.1210/er.2005-0888.
[30] M.B. Hoppa, S. Collins, R. Ramracheya, L. Hodson, S. Amisten, Q. Zhang, P. Johnson, F.M. Ashcroft, P. Rorsman, Chronic palmitate exposure inhibits insulin secretion by dissociation of $Ca^{2+}$ channels from secretory granules, Cell Metab. 10 (2009) 455–465, https://doi.org/10.1016/j.cmet.2009.09.011.
[31] Z. Gao, J. Reavey-Cantwell, R.A. Young, P. Jegier, B.A. Wolf, Synaptotagmin III/VII isoforms mediate $Ca^{2+}$-induced insulin secretion in pancreatic islet beta -cells, J. Biol. Chem. 275 (2000) 36079–36085, https://doi.org/10.1074/jbc.m004284200.
[32] J. Herrington, Y.P. Zhou, R.M. Bugianesi, P.M. Dulski, Y. Feng, V.A. Warren, M. M. Smith, M.G. Kohler, V.M. Garsky, M. Sanchez, M. Wagner, K. Raphaelli, P. Banerjee, C. Ahaghotu, D. Wunderler, B.T. Priest, J.T. Mehl, M.L. Garcia, O. B. McManus, G.J. Kaczorowski, R.S. Slaughter, Blockers of the delayed-rectifier potassium current in pancreatic beta-cells enhance glucose-dependent insulin secretion, Diabetes 55 (2006) 1034–1042, https://doi.org/10.2337/diabetes.55.04.06.db05-0788.
[33] M. Braun, R. Ramracheya, M. Bengtsson, Q. Zhang, J. Karanauskaite, C. Partridge, P.R. Johnson, P. Rorsman, Voltage-gated ion channels in human pancreatic beta-cells: electrophysiological characterization and role in insulin secretion, Diabetes 57 (2008) 1618–1628, https://doi.org/10.2337/db07-0991.
[34] R.T. Kennedy, L. Huang, M.A. Atkinson, P. Dush, Amperometric monitoring of chemical secretions from individual pancreatic beta-cells, Anal. Chem. 65 (1993) 1882–1887, https://doi.org/10.1021/ac00062a012.
[35] L. Huang, H. Shen, M.A. Atkinson, R.T. Kennedy, Detection of exocytosis at individual pancreatic beta cells by amperometry at a chemically modified microelectrode, Proc. Natl. Acad. Sci. U. S. A. 92 (1995) 9608–9612, https://doi.org/10.1073/pnas.92.21.9608.
[36] P.A. Smith, M.R. Duchen, F.M. Ashcroft, A fluorimetric and amperometric study of calcium and secretion in isolated mouse pancreatic beta-cells, Pflugers Arch 430 (1995) 808–818, https://doi.org/10.1007/BF00386180.
[37] L. Eliasson, E. Renström, W.G. Ding, P. Proks, P. Rorsman, Rapid ATP-dependent priming of secretory granules precedes $Ca^{2+}$-induced exocytosis in mouse pancreatic B-cells, J. Physiol. 503 (2) (1997) 399–412, https://doi.org/10.1111/j.1469-7793.1997.399bh.x. Pt.
[38] M. Ferdaoussi, X. Dai, M.V. Jensen, R. Wang, B.S. Peterson, C. Huang, O. Ilkayeva, N. Smith, N. Miller, C. Hajmrle, A.F. Spigelman, R.C. Wright, G. Plummer, K. Suzuki, J.P. Mackay, M. van de Bunt, A.L. Gloyn, T.E. Ryan, L.D. Norquay, M. J. Brosnan, J.K. Trimmer, T.P. Rolph, R.G. Kibbey, J.E. Manning Fox, W. F. Colmers, O.S. Shirihai, P.D. Neufer, E.T.H. Yeh, C.B. Newgard, P.E. MacDonald, Isocitrate-to-SENP1 signaling amplifies insulin secretion and rescues dysfunctional β cells, J. Clin. Invest. 125 (2015) 3847–3860, https://doi.org/10.1172/JCI82498.
[39] H.P. Meissner, Electrophysiological evidence for coupling between beta cells of pancreatic islets, Nature 262 (1976) 502–504, https://doi.org/10.1038/262502a0.
[40] P.E. MacDonald, P. Rorsman, Oscillations, intercellular coupling, and insulin secretion in pancreatic beta cells, PLoS Biol. 4 (2006), https://doi.org/10.1371/journal.pbio.0040049 e49.
[41] Q.F. Wan, Y. Dong, H. Yang, X. Lou, J. Ding, T. Xu, Protein kinase activation increases insulin secretion by sensitizing the secretory machinery to $Ca^{2+}$, J. Gen. Physiol. 124 (2004) 653–662, https://doi.org/10.1085/jgp.200409082.

[42] E. Renström, L. Eliasson, P. Rorsman, Protein kinase A-dependent and -independent stimulation of exocytosis by cAMP in mouse pancreatic B-cells, J. Physiol. 502 (1997) 105–118, https://doi.org/10.1111/j.1469-7793.1997.105bl.x (Pt 1).
[43] W.J. Song, P. Mondal, Y. Li, S.E. Lee, M.A. Hussain, Pancreatic β-cell response to increased metabolic demand and to pharmacologic secretagogues requires EPAC2A, Diabetes 62 (2013) 2796–2807, https://doi.org/10.2337/db12-1394.
[44] M. Shigeto, R. Ramracheya, A.I. Tarasov, C.Y. Cha, M.V. Chibalina, B. Hastoy, K. Philippaert, T. Reinbothe, N. Rorsman, A. Salehi, W.R. Sones, E. Vergari, C. Weston, J. Gorelik, M. Katsura, V.O. Nikolaev, R. Vennekens, M. Zaccolo, A. Galione, P.R.V. Johnson, K. Kaku, G. Ladds, P. Rorsman, GLP-1 stimulates insulin secretion by PKC-dependent TRPM4 and TRPM5 activation, J. Clin. Invest. 125 (2015) 4714–4728, https://doi.org/10.1172/JCI81975.
[45] A. Tengholm, E. Gylfe, cAMP signalling in insulin and glucagon secretion, Diabetes Obes. Metab. 19 (1) (2017) 42–53, https://doi.org/10.1111/dom.12993. Suppl.
[46] R.A. Easom, CaM kinase II: a protein kinase with extraordinary talents germane to insulin exocytosis, Diabetes 48 (1999) 675–684, https://doi.org/10.2337/diabetes.48.4.675.
[47] I. Dzhura, O.G. Chepurny, C.A. Leech, M.W. Roe, E. Dzhura, X. Xu, Y. Lu, F. Schwede, H.G. Genieser, A.V. Smrcka, G.G. Holz, Phospholipase C-ε links Epac2 activation to the potentiation of glucose-stimulated insulin secretion from mouse islets of Langerhans, Islets 3 (2011) 121–128, https://doi.org/10.4161/isl.3.3.15507.
[48] J.E. Richmond, R.M. Weimer, E.M. Jorgensen, An open form of syntaxin bypasses the requirement for UNC-13 in vesicle priming, Nature 412 (2001) 338–341, https://doi.org/10.1038/35085583.
[49] E.P. Kwan, L. Xie, L. Sheu, C.J. Nolan, M. Prentki, A. Betz, N. Brose, H.Y. Gaisano, Munc13-1 deficiency reduces insulin secretion and causes abnormal glucose tolerance, Diabetes 55 (2006) 1421–1429, https://doi.org/10.2337/db05-1263.
[50] L. Kang, Z. He, P. Xu, J. Fan, A. Betz, N. Brose, T. Xu, Munc13-1 is required for the sustained release of insulin from pancreatic beta cells, Cell Metab 3 (2006) 463–468, https://doi.org/10.1016/j.cmet.2006.04.012.
[51] D.D. MacDougall, Z. Lin, N.L. Chon, S.L. Jackman, H. Lin, J.D. Knight, A. Anantharam, The high-affinity calcium sensor synaptotagmin-7 serves multiple roles in regulated exocytosis, J. Gen. Physiol. 150 (2018) 783–807, https://doi.org/10.1085/jgp.201711944.
[52] N. Gustavsson, Y. Lao, A. Maximov, J.C. Chuang, E. Kostromina, J.J. Repa, C. Li, G. K. Radda, T.C. Südhof, W. Han, Impaired insulin secretion and glucose intolerance in synaptotagmin-7 null mutant mice, Proc. Natl. Acad. Sci. U. S. A. 105 (2008) 3992–3997, https://doi.org/10.1073/pnas.0711700105.
[53] S. Dolai, L. Xie, D. Zhu, T. Liang, T. Qin, H. Xie, Y. Kang, E.R. Chapman, H. Y. Gaisano, Synaptotagmin-7 functions to replenish insulin granules for exocytosis in human islet β-cells, Diabetes 65 (2016) 1962–1976, https://doi.org/10.2337/db15-1436.
[54] T. Bacaj, D. Wu, X. Yang, W. Morishita, P. Zhou, W. Xu, R.C. Malenka, T.C. Südhof, Synaptotagmin-1 and synaptotagmin-7 trigger synchronous and asynchronous phases of neurotransmitter release, Neuron 80 (2013) 947–959, https://doi.org/10.1016/j.neuron.2013.10.026.
[55] P.E. MacDonald, S. Obermüller, J. Vikman, J. Galvanovskis, P. Rorsman, L. Eliasson, Regulated exocytosis and kiss-and-run of synaptic-like microvesicles in INS-1 and primary rat beta-cells, Diabetes 54 (2005) 736–743, https://doi.org/10.2337/diabetes.54.3.736.
[56] M. Schaefer, N. Albrecht, T. Hofmann, T. Gudermann, G. Schultz, Diffusion-limited translocation mechanism of protein kinase C isotypes, FASEB J 15 (2001) 1634–1636, https://doi.org/10.1096/fj.00-0824fje.
[57] S. Barg, C.S. Olofsson, J. Schriever-Abeln, A. Wendt, S. Gebre-Medhin, E. Renström, P. Rorsman, Delay between fusion pore opening and peptide release from large dense-core vesicles in neuroendocrine cells, Neuron 33 (2002) 287–299, https://doi.org/10.1016/S0896-6273(02)00563-9.
[58] A. Kogel, H. Kalwa, N. Urban, M. Schaefer, Artifact-free objective-type multicolor total internal reflection fluorescence microscopy with light-emitting diode light sources-Part I, J. Biophotonics 12 (2019) e201900033, https://doi.org/10.1002/jbio.201900033.
[59] M. Schaefer, H. Kalwa, Theoretical background of light-emitting diode total internal reflection fluorescence microscopy and photobleaching lifetime analysis of membrane-associated proteins-Part II, J. Biophotonics 13 (2020) e201960181, https://doi.org/10.1002/jbio.201960181.
[60] G. Miesenböck, D.A. de Angelis, J.E. Rothman, Visualizing secretion and synaptic transmission with pH-sensitive green fluorescent proteins, Nature 394 (1998) 192–195, https://doi.org/10.1038/28190.